RMP Enhanced Transport and Rotation Screening in DIII-D Simulations

V.A. Izzo 1), I. Joseph 2), R.A. Moyer 1), T.E. Evans 3), M.E. Fenstermacher 2),
T.H. Osborne 3), L.L. Lao 3), and P.B. Snyder 3)

1) University of California, San Diego, California, USA
2) Lawrence Livermore National Lab, Livermore, California, USA
3) General Atomics, San Diego, California, USA

e-mail contact of main author: izzo@fusion.gat.com

Abstract. The application of resonant magnetic perturbations (RMP) to DIII-D plasmas at low collisionality has achieved ELM suppression, primarily due to a pedestal density reduction. The mechanism of the enhanced particle transport is investigated in 3D MHD simulations with the NIMROD code. The simulations apply realistic vacuum fields from the DIII-D I-coils, C-coils and measure intrinsic error fields to an EFIT reconstructed DIII-D equilibrium, and allow the plasma to respond to the applied fields while the fields are fixed at the boundary, which lies in the vacuum region. A non-rotating plasma amplifies the resonant components of the applied fields by factors of 2-5. The poloidal velocity forms E×B convection cells crossing the separatrix, which push particles into the vacuum region and reduce the pedestal density. Low toroidal rotation at the separatrix reduces the resonant field amplitudes, but does not strongly affect the particle pump-out. At higher separatrix rotation, the poloidal E×B velocity is reduced by half, while the enhanced particle transport is entirely eliminated. A high collisionality DIII-D equilibrium with an experimentally measured rotation profile serves as the starting point for a simulation with odd parity I-coil fields that can ultimately be compared with experimental results. All of the NIMROD results are compared with analytic error field theory.

1. Introduction

The edge localized modes (ELMs) that can occur in ITER H-mode operation have the potential to damage the plasma facing components due to large intermittent heat fluxes [1]. Experiments on the DIII-D device have sought a method of reducing or eliminating ELMs with the use of non-axisymmetric resonant magnetic perturbations (RMPs) generated by the so-called I-coils [2-4]. Typically fields with n=3 toroidal symmetry are used, with both odd and even up-down symmetries. Experiments with even parity I-coil fields in low collision-ality plasmas have effectively eliminated ELMs by reducing the pedestal pressure gradient below the stability threshold. However, the pressure pedestal reduction comes mainly in the form of an edge density reduction, while the temperature is less significantly impacted, despite the large enhanced heat flux that would be expected in the presence of ergodic fields [5,6]. Several mechanisms for the enhanced particle transport are possible, including E×B convection, which will be considered here in the context of MHD simulations.

Further DIII-D experiments have significantly reduced ELM amplitudes with the application of odd parity I-coil fields in more collisional plasmas [2]. In these experiments, little or no change in the pedestal pressure is observed. Thus, the RMP fields may interact directly with the ELMs and not merely with the 2D stability. The specific mechanism of the ELM reduction is not known, but it may be best explored by means of 3D nonlinear MHD simulations.

Fitzpatrick [7,8] provides an analytic theory for the penetration of error fields in a rotating tokamak. First, an equilibrium which is marginally tearing stable at a particular resonant sur-face will amplify an applied resonant error field. This is an ideal effect, dependent only on the tearing stability parameter Δ′. Second, rotation at the resonant surface will screen the applied fields, reducing or eliminating the particular resonant component everywhere inside the resonant surface. Although the theory applies strictly to a straight periodic cylinder, we

will compare the results of MHD simulations in real geometry to the analytic theory where possible.

2. Numerical Model

The numerical simulations presented here are performed with the MHD code NIMROD [9], using a resistive MHD model. The simulations begin with two EFIT reconstructed DIII-D equilibria from shots 113317 and 119690. Shot 113317 was not an RMP experimental discharge, but has been used in previous peeling-ballooning mode computations with NIMROD [10]. Here, even parity I-coil fields are applied to the equilibrium, although this is a higher collisionality shot than typical even parity I-coil experiments. Measured density and temperature profiles are used, but the imposed rotation profiles are artificial. Shot 119690 is from an odd I-coil RMP experiment, and is used as the starting point for odd I-coil simulations. In those simulations, the experimentally measured density, temperature, and rotation profiles are used.

In each simulation, the vacuum RMP fields associated with the appropriate coil currents are superimposed on the 2D equilibrium fields as an initial condition. Thus, the simulations begin with fully penetrated RMP fields, which differs from the experimental conditions of ramping the I-coil currents from zero in the presence of the tokamak plasma. The plasma evolves to a saturated 3D equilibrium state, subject to constant vacuum field values at the boundary. However, it should be noted that such a system can have hysteresis [7], wherein the initial condition determines the final saturated state. The simulation boundary is located outside of the separatrix, so that a small vacuum region is included, and the RMP boundary conditions are fixed outside of that vacuum region. In addition to the I-coil fields, the measured error fields, plus the n=1 C-coil fields that are used to correct the error fields are included in the initial condition.

The model is limited for numerical reasons by the inability to match the experimental plasma dimensionless parameters. For computational expediency, the Lundquist number, S, is reduced in each case by enhancing the plasma resistivity above the Spitzer value by factors of 10–100. This results in simulated Lundquist numbers of 10^5-5×10^6 for the two equilibria. The plasma kinematic viscosity is also enhanced to a value of 100 m^2/s in each case. The heat transport is strongly anisotropic, with $\kappa_\parallel/\kappa_\perp = 10^8$, but the parallel heat flux is still on the order of 100 times smaller than experimental values.

3. Simulation Results

The results of five NIMROD simulations are presented. Three have even I-coil fields and differ only in terms of toroidal rotation profile. The remaining two simulations with odd I-coil fields have identical rotation profiles, but different Lundquist numbers.

3.1 Shot 113317 with Even Parity I-Coils

The first of three even I-coil simulations has no toroidal rotation, while each of the other two has a core rotation velocity of about 100 km/s (9.4 kHz). One simulation, referred to as the "high rotation" simulation, has separatrix rotation velocity of 35 km/s (3.3 kHz), while the other, referred to as the "low rotation" simulation, has a separatrix velocity of about 1 km/s (94 Hz). The two rotation profiles are seen in Fig. 1. The reconnection time in these simulations is on the order of 0.1 ms, with each simulation being run for several times that duration. The magnetic fields therefore come to an approximate steady state. However, the transport timescales are much longer than the simulation duration, thus only the initial effects

of the changes in transport can be observed, but no steady state is achieved. The applied fields correspond to an I-coil current of 3 kA.

In Fig. 2 is shown puncture plots of the final magnetic field configuration for each of the 3 simulations. A large stochastic region appears at the edge of the non-rotating simulations, which extends to smaller minor radius than even the stochastic region generated by the initial

FIG. 1. The two rotation profiles used in the even parity I-coil simulations.

vacuum fields. In the low rotation simulation, the width of the stochastic region narrows, and there is also a reduction of the width of the central 1/1 island, which is induced by the C-coil and error fields. The high rotation simulation has mostly good flux surfaces, with only a small amount of edge stochasticity. The 1/1 island, however, is more comparable in width to the non-rotating simulation.
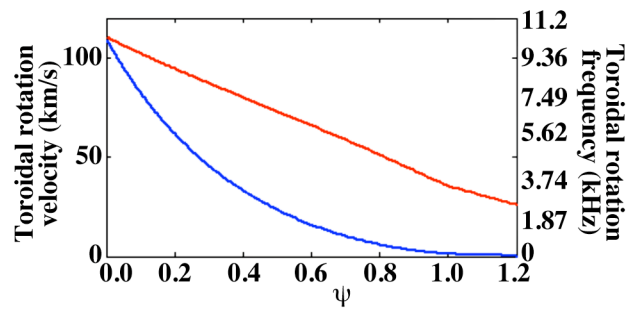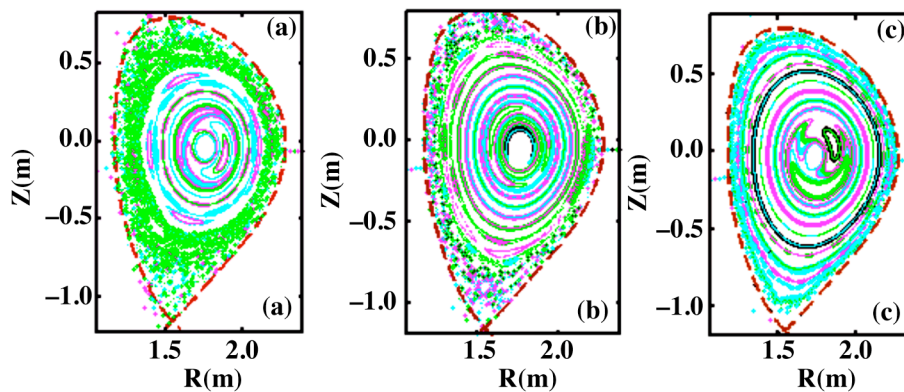

FIG. 2. Puncture plots of the magnetic field in the saturated steady-state configuration with (a) no rotation, (b) low rotation, and (c) high rotation.

For each case, the n=3 component of the magnetic fields is transformed into straight-field-line coordinates, and is spectrally decomposed in the poloidal direction. The result is seen in Fig. 3, showing the normal (to the flux surface) component of the n=3 magnetic field, as a function of the poloidal flux coordinate, ψ, and the poloidal mode number m. The fields in each case are plotted at the maximum phase, which can change from the vacuum phase due to rotation. In particular, the vacuum fields are a maximum at a phase of $\pi/2$, while the high rotation simulation has a phase maximum of 0.3π. The even I-coil fields have strong resonant components. When these resonant fields are amplified by the plasma response, they can become the dominant fields, as seen in the figure, particularly in the non-rotating case. In the high rotation case, the symmetry of the fields across the resonant time changes relative to the other two simulations.

According to Fizpatrick [7,8], the reconnected flux at a particular resonant surface (Ψ_s) is related to the imposed vacuum flux (Ψ_v) by the formula:

$$\Psi_s = \frac{2m}{-\Delta' + \Delta(\omega)} \Psi_v \quad .$$

(1)

Here, Δ' is the tearing stability index at the resonant surface, and $\Delta(\omega)$ is the dissipative boundary layer response to the applied error field near the rational surface. The frequency ω is the toroidal mode number, n, times the plasma rotation frequency. At zero rotation, the Δ' term in the denominator amplifies applied resonant fields in marginally stable cases where $\Delta' < 2 m$. Rotation acts to reduce the mode amplitude by screening. We can calculate both Ψ_s and Ψ_v for each poloidal m component of the n=3 fields for the saturated state in the three simulations (Fig. 4). However, the theory has the value of the applied fields held fixed at the separatrix. In the simulations, the fields are held fixed outside the vacuum region, which is not treated as a true vacuum region by NIMROD. Thus, the final state has different fields at the separatrix, which determine the true vacuum fields that should be used for the comparison. Thus, each resonant component is rescaled so that the vacuum value and the plasma value match at the separatrix. At zero rotation, nearly all of the resonant components are amplified by the plasma; the non-resonant components are unaffected. As the rotation is increased, the mode amplitudes decrease. In the high rotation case, most of the n=3 resonant component amplitudes are below the vacuum values, explaining the considerable healing of flux surfaces.

Though the Fitzpatrick theory only strictly applies to a straight cylinder, if we assume that it is descriptive of the NIMROD results, then we can estimate the value of Δ' at each resonant surface from the amplification in the non-rotating case. With this result, we can test the screening portion of the theory by calculating the theoretical $\Delta(\omega)$ for the two rotation profiles. We use the expression for $\Delta(\omega)$ in the visco-resistive regime from Ref. [7], to obtain the screening factors in Fig. 5. If we combine these theoretical screening factors with Δ' estimates we can obtain a predicted mode amplitude for each n=3 component. These are compared with the actual mode amplitudes in Fig. 5. For both rotation profiles, the actual amplitudes are considerably larger than the predicted amplitudes for nearly all modes.
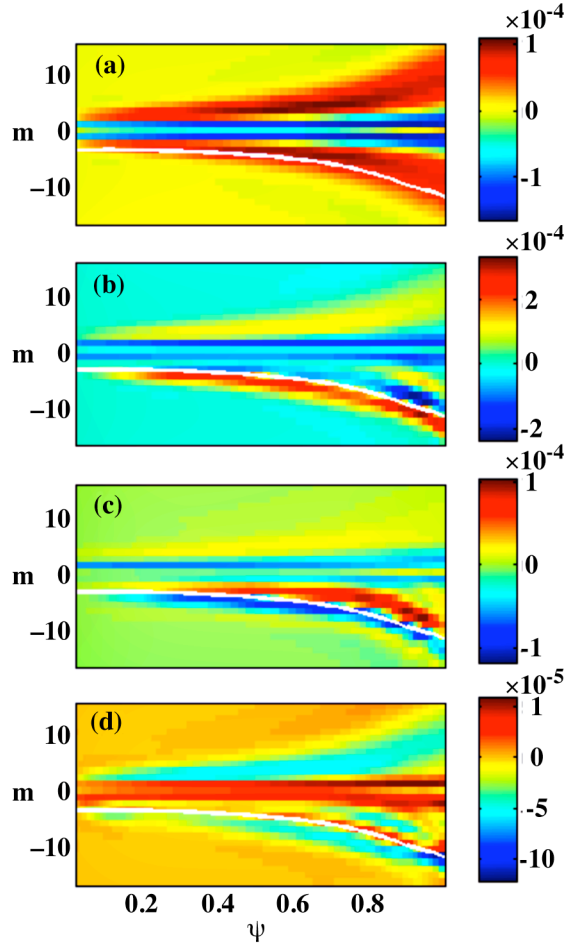

FIG. 3. The normal (to the flux surface) component of the n=3 magnetic field in straight field line coordinates, as a function of the poloidal flux coordinate and poloidal mode number for (a) the vacuum fields, and plasma response with (b) no rotation, (c) low rotation, and (d) high rotation.
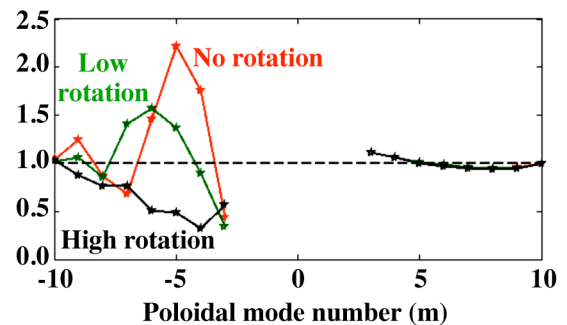

FIG. 4. The ratio of the n=3 reconnected flux to the vacuum flux (Ψ_s/Ψ_v) for each poloidal mode number m. Negative m are the resonant modes, while positive m are non-resonant.

In no-rotation and low rotation simulations, the pedestal density decreases. This occurs as a result of n=3 E×B convection cells that cross the separatrix and push particles into the vacuum region. In the high rotation case, these cells appear with reduced velocity, but no enhanced density transport occurs. The final density profiles are shown in Fig. 6, along with the normal component of the n=3 velocity along the separatrix. The peak velocity is 400 m/s, which must be compared with other density transport mechanisms to determine if this mechanism will be dominant or even significant. However, as resistivity decreases, the E×B velocity will decrease, so the result must be scaled appropriately to the relevant tokamak regime.

FIG. 5. The ratio of resonant flux over the vacuum flux for each case from the NIMROD runs (dashed curves) and the predicted screened solution using the theoretical screening factors and the amplification from the non-rotating simulation (solid curves).
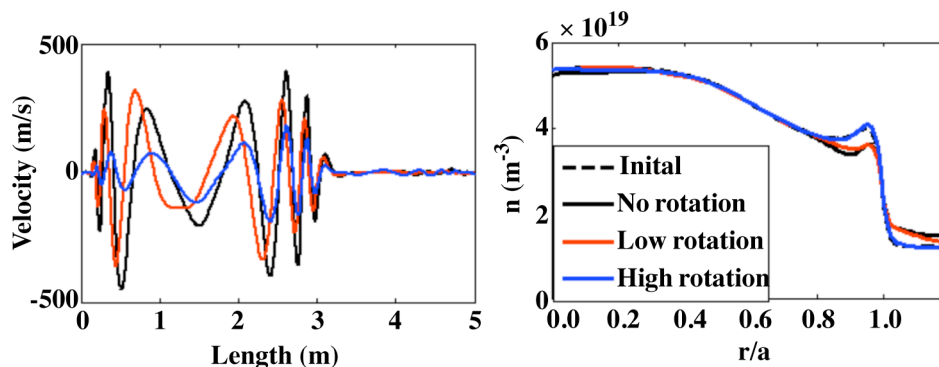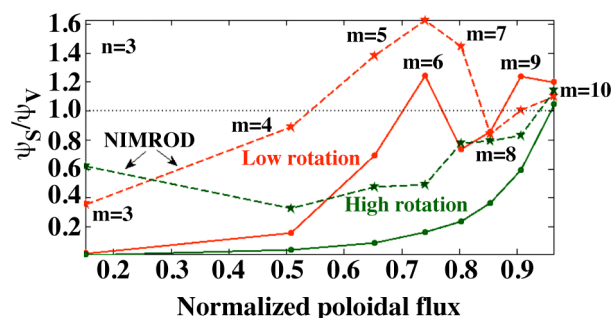

FIG. 6. (Left) The normal (to the separatrix) n=3 velocity along the separatrix, starting at the X-point, and moving along the outboard and then the inboard sides. (Right) The final density profiles for each of the three even I-coil simulations.

3.2 Shot 119690 with Odd Parity I-Coils

The second set of simulations was performed with an equilibrium from shot 119690 with an experimentally measured rotation profile of about 80 km/s in the core and 20 km/s at the separatrix. The I-coil current is 4.35 kA, corresponding to the actual experiment, in which odd parity I-coil fields were used to reduce ELMs in a high collisionality plasma. The Lundquist number of the experimental discharge is 5×10^7. The two simulations differ only in terms of the resistivity, which is enhanced by a factor of 10 above Spitzer in one case, and a factor of 100 in the other case, giving $S=5 \times 10^6$ and $S=5 \times 10^5$ respectively. Despite the larger I-coil currents than in the previous simulations, the odd parity fields are mostly non-resonant and do not perturb the flux surfaces as significantly.

In Fig. 7 is plotted the ratio of the reconnected flux from the saturated states of the two simulations Ψ_s and the vacuum resonant n=3 components Ψ_v. The applied resonant components fall off toward the center of the plasma much more so than in the even parity situation. The majority of the n=3 components are reduced in the higher S simulation relative to the lower S case. This is consistent with the screening theory, which becomes more effective at

lower resistivity. In particular, in the visco-resistive regime, the screening parameter $\Delta(\omega)$ scales as $\eta^{-5/6}$. If we consider Δ and Δ' as unknowns in Eq. (1), and use the known resistivity scaling, we can arrive at two equations with two unknowns for these two simulations, where Ψ_s/Ψ_v are taken from the NIMROD results. Assuming the results are consistent with the theory, this approach should yield estimates for both Δ and Δ' at each resonant surface. These estimates are plotted in Fig. 8. The estimates for Δ' resemble closely the Δ' estimates obtained from the no-rotation

FIG. 7. The ratio of the n=3 reconnected flux to the vacuum flux (Ψ_s/Ψ_v) for each poloidal mode number m in the odd parity I-coil simulations.

simulation (for the 113317 equilibrium). Namely, the highest and lowest m components fall in the amplified regime -$\Delta' < 2$ m), while the intermediate modes (m~8) are not amplified in the ideal case. The estimates for $\Delta(\omega)$ are plotted in terms of the associated screening factor for no amplification. The trends do not match the appropriate scaling with resistivity, rotation velocity, etc. The calculation assumes that $\Delta(\omega)$ is purely imaginary, which is true for the visco-resistive regime, but in the case of m=3 and m=8, the assumption fails. The screening factor that exceeds unity in those two cases is indicative of the failure of the model. Clearly, the higher mode amplitudes in the higher S case for these two m are not consistent with the theory. In these simulations, no change in the density profile occurs.
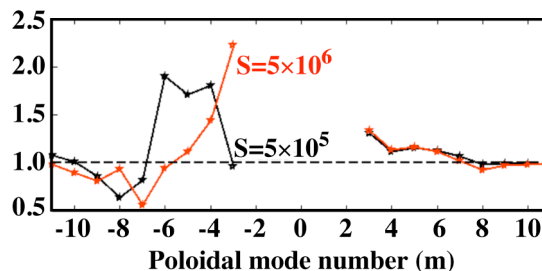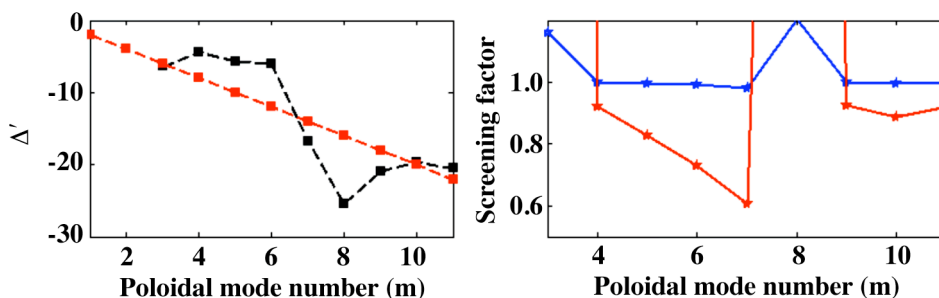

FIG. 8. (Left) The estimate for Δ' from the odd I-coil simulations (black), and the line $\Delta' = -2$ m (red). (Right) The estimated screening factor from the odd I-coil simulations in the S=5×10^6 (red) and S=5×10^5 (blue) runs.

4. Conclusions

Both even and odd I-coil parity simulations have been performed with NIMROD and considered in light of the Fitzpatrick error field theory. In the case of even parity, the experimentally observed effect of a density pump-out occurs in the simulations, although sufficiently high separatrix rotation eliminates this effect. The E×B flow responsible for the particle transport will likely decrease in amplitude with decreasing resistivity, where a linear scaling is suggested [11]. With a peak velocity of 400 m/s, a factor of 100 reduction would render this mechanism small relative to parallel outflow estimates for DIII-D on the order of 15 m/s [12]. Thus, the dominant mechanism in realistic DIII-D plasmas needs further exploration.

Comparison of the mode amplitudes with theoretical predictions is not in complete agreement in either the odd or even parity simulations. In particular, the simulated screening of the resonant modes appears much less effective than the analytic theory predicts. With

toroidal effects neglected in the theory, the toroidal coupling of modes at various resonant surfaces may be the primary culprit. Furthermore, the theory we have considered described only the linear response of the plasma to the applied error fields, whereas nonlinear effects come into play in the NIMROD simulations. The benefit of accurately predicting the scaling of each resonant mode amplitude with rotation and resistivity would be the ability to reconstruct the predicted fields for any plasma resistivity and rotation profile without running the NIMROD simulation.

Acknowledgments

References

[1]   ITER Physics Basis Editors, ITER Physics Expert Group, and ITER Joint Central Team and Physics Integration Unit, Nucl. Fusion **39**, 2137 (1999).
[2]   EVANS, T.E., *et al.*, J. Nucl. Mater. **337-339**, 691 (2005).
[3]   BURRELL, K.H., *et al.*, Plasma Phys. Control. Fusion **47**, B37 (2005).
[4]   EVANS, T.E., *et al.*, Phys. Plasmas **13**, 056121 (2006).
[5]   JOSEPH, I., *et al.*, J. Nucl. Mater. **363-365**, 598 (2007).
[6]   JOSEPH, I., *et al.*, Nucl. Fusion **48**, 045009 (2008).
[7]   FITZPATRICK, R., Phys. Plasmas **5**, 3325 (1998).
[8]   FITZPATRICK, R., *et al.*, Nucl. Fusion **33**, 1049 (1993).
[9]   SOVINEC, C.R., *et al.*, J. Computational Phys. **195,** 355 (2004).
[10]   PANKIN, A.Y., *et al.*, Plasma Phys. Control. Fusion **49**, S63 (2007).
[11]   NARDON, E., *et al.,* Phys. Plasmas **14**, 092501 (2007).
[12]   TOKAR, M.Z., *et al.,* Nucl. Fusion **48**, 024006 (2008).